The Spatial Structure of the Solar Wind and Comparisons with Solar Data and Models

M. Neugebauer[1], R. J. Forsyth[2], A. B. Galvin[3], K. L. Harvey[4], J. T. Hoeksema[5], A. J. Lazarus[6], R. P. Lepping[7], J.A. Linker[8], Z. Mikic[8], J. T. Steinberg[6], R. von Steiger[9], Y.-M. Wang[10], and R. F. Wimmer-Schweingmber[11]

1. Jet Propulsion Laboratory, California Institute of Technology, Pasadena
2. Blackett Laboratory, Imperial College, London
3. University of Maryland, College Park
4. Solar Physics Research Corp., Tucson
5. Center for Space Science and Astronomy, Stanford, CA
6. Center for Space Research, Massachusetts Institute of Technology, Cambridge
7. NASA Goddard Space Flight Center, Greenbelt, MD
8. Science Applications International Corp, San Diego
9. International Space Science Institute, Bern
10. Naval Research Laboratory, Washington, DC
11. Physikalisches Institut, University of Bern

Abstract. Data obtained by instruments on the Ulysses spacecraft during its rapid sweep through >90° of solar latitude, crossing the solar equator in early 1995, were combined with data obtained near Earth by the WIND spacecraft to study the spatial structure of the solar wind and to compare with different models of the interplanetary field derived from solar observations. Several different source-surface models matched the double sinusoidal structure of the heliospheric current sheet (HCS), but with differences in latitude as great as 210. The source-surface model that included an interplanetary current sheet gave poorer agreement with observed current sheet crossings during this period than did the other source surface models or an MHD model. A best fit between the calculated and observed locations of the HCS was obtained by adding 22° of solar rotation to the constant-velocity travel time from the source surface to the spacecraft. The photospheric footpoints of the open field lines calculated from the models generally agreed with observations in the He 10830 Å line of the locations of coronal holes, with the exceptions that (1) in some places, open field lines originated outside the coronal hole boundaries and (2) the models show apparently closed-field regions just inside some coronal hole boundaries. The patterns of mismatches between coronal hole boundaries and the envelopes of open field lines persisted over at least three solar rotations. The highest speed wind came from the polar coronal holes, with the wind originating deeper within the hole being faster than the wind coming from near the hole boundary. Intermediate and slow streams originated in smaller coronal holes at low latitudes and from open field regions just outside coronal hole boundaries. Although the HCS threaded regions of low speed, low helium abundance, high ionization temperature, and a high ratio of magnesium to oxygen densities (a surplus of an element with low first ionization potential), there was a great deal of variation in these parameters from one place to another along the HCS. The gradient of speed with latitude varied from 14 to 28 km/s/deg.

Introduction

In July, 1996, the International Space Science Institute in Bern, Switzerland, sponsored a meeting of the Inter-Agency Consultative Group (IACG) Campaign IV, Solar Sources of Heliospheric Structure Observed Out of the Ecliptic. The week-long meeting brought together people who view the Sun from the Yohkoh and SOHO spacecraft and from the ground, representatives of solar wind and magnetic field experiments on the WIND and Ulysses spacecraft, and theoreticians with experience in modeling the solar wind and the interplanetary magnetic field, Participants accessed their data or models electronically for on-the-spot comparisons. Different models were compared to each other, to observations of coronal holes on the Sun, and to the solar wind and interplanetary fields observed at WIND and Ulysses. Because of the relative stability of the Sun during the several months centered on the rapid passage of Ulysses from high southerly through equatorial to high northerly latitudes, it was also possible to construct latitude-longitude maps of the field and plasma parameters during this era. The meeting participants felt the insights gained by these exchanges were worth sharing with the broader community. We have therefore expanded and improved the data base, modified many of the plot formats, and present the results of the comparisons together with some discussion here.

Trajectories and Sources of Spacecraft Data

The analysis in this paper is based on ion and magnetic field parameters observed by the Ulysses and WIND spacecraft. The Ulysses proton and alpha-particle data were obtained by the SWOOPS experiment [*Bame et al.*, 1992], the magnetic field data were obtained by the vector helium magnetometer [*Balogh et al.*, 1992], and the heavy ion data were obtained by the SWICS experiment [*Gloeckler et al.*, 1992]. For WIND, the plasma and field data were obtained by the S WE and MFI instruments [*Ogilvie et al.*, 1995;

Lepping et al., 1995], respectively. The present analyses are based on one- or three-hour averages of the in situ data.

In its passage from the southern to the northern hemisphere, the Ulysses spacecraft crossed the heliographic equator on March 5, 1995, at a solar distance of 1.34 AU. Some of the principal findings of this "fast-latitude scan" are summarized by *Smith and Marsden [1995]*. Figure 1 provides a map of the latitudes and Carrington longitudes of the mapped-back locations on the solar surface of the solar wind observed at Ulysses and WIND during this interval calculated from the observed speeds assuming constant-speed radial flow between the Sun and the spacecraft. Although for most of this paper we concentrate on data obtained during Barrington rotations (CR) 1892-1894, some data from CR 1891 and 1895 are also used. During this five-rotation interval (Dee 13, 1994- May 15, 1995), the WIND spacecraft was located sunward of the Earth at a geocentric distance ranging from 100 to 250 Earth radii. The heliographic latitude and longitude of WIND during CR 1892-4, shown in Figure 1, indicate that WIND was near its annual southernmost (-7.25°) excursion in heliographic latitude.

During solar rotations 1892-1894 (Jan 27, 1995- Apr 19, 1995), Ulysses was on the far side of the Sun as seen from Earth. At the start of CR 1892, the source region of the plasma observed by Ulysses was located 55° behind the east limb of the Sun, while at the end of CR 1894, the Ulysses source region was 38° behind the west limb. Thus interpretation of the solar wind measured at Ulysses in terms of solar features observed from Earth, such as coronal hole boundaries or photospheric magnetic fields, is complicated unless the Sun and solar wind structure remained essentially static over periods of at least weeks. Fortunately, that was the case during the interval of interest because the Sun was in a state of very low activity. Two different types of evidence are presented in Figure 2. Figure 2a displays hourly averages of the solar wind speed observed by WIND versus time, on a 27-day scale, starting on day 30, 1995. The hours marked "CMIS" were

classified as transient solar wind resulting from coronal mass ejections on the basis of either magnetic cloud geometry, an unusually high helium abundance, or an interval identified as a CME by *Crooker et al. [1997]*. The same general pattern of two high-speed and two low-speed intervals was seen in each of the three rotations. Although the first high-speed stream observed during CR 1892 was temporally wider than it was in the following rotations, the edges of the other streams varied within a temporal envelope of ~±1 day, which corresponds to a spread of -*13° in solar longitude. The speeds within each fast and slow stream were constant from one rotation to the next within -8% and 15% for the high- and low-speed streams, respectively. The CME intervals are excluded from some of the analyses that follow, thereby removing the exceptionally low speeds seen near rotation day 10.

Another test for stability in the Sun and solar wind structure during the period being studied is to examine changes in the positions of the heliospheric current sheet (HCS) computed from observations of the photospheric field. Such data are shown in Figure 2b, which is a plot of the heliographic latitude and longitude of the HCS on a source surface at 2.5 solar radii (R_s) over CR 1891-5. The details of this and other models for the current sheet are discussed below. The point to be made from Figure 2b is that the general shape of the computed current sheet, roughly a double sinusoid, was constant throughout all five rotations, although at any longitude, the latitude varied over a range of *9* to 28°. Synoptic maps of coronal line emission observed at the east and west solar limbs by the Sacramento Peak coronagraph also remained quite stable during these five solar rotations (Solar-Geophysical Data Prompt Reports #608-61 2, April-August, 1995).

Figure 2 convinced us that the structure of the Sun and solar wind did not vary significantly during the period of the Ulysses fast latitude scan and that something useful could probably be learned by combining the Ulysses and WIND data over several solar rotations. In interpreting the results, however, it is necessary to remember that positional

variations of the order of 10-15° and speed differences of 10- 15% should not be taken seriously.

Comparison of Different Models

Several different methods have been devised for estimating the strength and direction of the interplanetary magnetic field, as well as the solar wind speed, from observations of the photospheric magnetic field, Many of them are based on the calculation of the field between the photosphere and a spherical surface, called the source surface, placed at several solar radii where the field is forced to be radial [*Schatten et al.*, 1969]. Within this general framework, there are many choices to be made. First, one has a choice of input data with differing spatial resolutions from several solar observatories. Then there is a question of whether or how the measured photospheric field should be corrected for the effect of saturation of the spectral line used for the measurement and/or for the strength of the poorly determined polar fields. One also has a choice of matching the calculated coronal field to the observed line-of-sight measurement versus assuming the field at the photosphere is purely radial and calculating that radial field from the line-of-sight component and the angular distance from the center of the disk. One must also choose the distance of the source surface from the Sun. Another approach is to include a current along the heliospheric current sheet outside the source surface [*Schatten*, 1971]. Still further refinements are being developed; *Zhao and Hoeksema [1995],* for example, describe a model with horizontal currents flowing near the Sun derived from magnetostatic calculations together with a cusp surface above which all the field lines are open as well as a source surface and a warped HCS.

Another approach which has been developed recently is to solve the three-dimensional magnetohydrodynamic (MHD) equations to determine the state of the coronal

plasma. In these calculations, the time-dependent MHD equations (conservation of mass, momentum, and energy, along with Ohm's law and Faraday's law) are solved until a steady state is established [*Mikic and Linker, 1996; Linker et al., 1996]*. In this model, closed and open coronal magnetic fields are determined self consistently along with the solar wind structure. The photospheric magnetic field is applied as a boundary condition, and the calculations can be extended from the Sun to 1 AU and beyond *[Linker and Mikic, 1997]*. In this paper we use a version of this model that simulates only the inner corona, between the photosphere and a radius of 20 R_s, using a polytropic energy equation.

Figure 3 depicts the differences in the location of the heliospheric current sheet derived from several choices of data, models, and parameters. CR 1892 was chosen for this comparison because it was the only rotation during the Ulysses fast latitude scan for which the data from the Wilcox Solar Observatory (WSO) are complete.

Figures 3a and 3b illustrate the effects of using data from different observatories processed by different people. The HCS locations in Figure 3a are calculated from a current-sheet (CS) model with the source surface at a heliocentric distance of 2.5 R_s and the field at the inner boundary (the solar surface) assumed to be radial. The curve marked WSO was calculated from measurements by the Wilcox Solar Observatory with a correction of the observed (saturated) intensity of the line-of-sight magnetic field by a factor $(4.5 - 2.5 \sin^2\lambda)$ where λ is solar latitude *[Wang and Sheeley, 1995]*. The curve marked NSO was calculated from observations by the National Solar Observatory/Kitt Peak which includes different corrections which are described in a document available at http://www.nso.noao.edu/kpvt/synoptic/README. Use of the two different data sources results in latitudinal differences $\leq 10°$, which is only twice the digitization step size of 5°.

The HCS locations shown in Figure 3b are based on a source-surface (SS) model, again with the source surface placed at 2.5 R_s and a radial boundary condition, but without

a current sheet. The three curves are based on magnetograph data obtained and processed by NSO and on WSO data processed independently by Wang and by Hoeksema. Again, the differences between the models using two different sets of input data are $\leq 10°$ in latitude at any longitude.

Comparison of Figure 3a with Figure 3b reveals that the HCS computed with the current sheet model is much flatter than the HCS computed with the source-surface model without a current sheet. The flatness of the HCS in the current-sheet model is probably due to the fact that the higher-order magnetic multiples (including the nonaxisymmetric quadruple component, which was quite substantial at this time) continue to fall off outside *2.5* R_s, whereas in the source-surface model without a current sheet, the field lines are radial beyond 2.5 R_s. For a more detailed discussion, see *Wang [* 1996].

The Wilcox Solar Observatory at Stanford University provides two different models of the coronal magnetic field on-line at http://quake.stanford.edu/~wso/coronal.html. These are the "Classic" and the "Radial" models. 'I'he on-line Radial model differs from that plotted in Figure 3b in that its source surface is placed at *3.25* rather than 2.5 R_s. The value of 3.25 R_s was chosen to fit the location of the HCS observed by Ulysses in 1991. Figure *3C* illustrates the effect of changing the source surface distance from 3.25 to 2.5 R_s; the effect is relatively small for the particular solar-minimum conditions studied here.

Comparison of Figures 3a and 3C shows that the HCS computed from the Radial model has about the same amplitude or flatness as the current-sheet model, but is displaced about 10° to the south. A possible reason for the southward displacement is that the photospheric field contains a strong axisymmetric (ℓ = 2, m = O) quadrupole component. A detailed discussion may be found in *Wang [1996];* see especially Figure 5b in that paper, which shows a southward displacement of the model neutral line for CR 1868.

Figure 3d compares the source-surface and current-sheet models calculated using the methods of *Wang and Sheeley [1995]* (W&S) to models used by the Stanford group. Because the coronal fields based on the "Classic" model [*Hoeksema et al.,* 1983] are available on-line starting in May 1976, they have been used in many studies. The Classic model is based on data from WSO, no saturation correction but a significant polar field correction, a line-of-sight boundary condition, and a source-surface at 2.5 R_s.; it has been optimized to match the polarity of the interplanetary magnetic field (IMF) at Earth over an extended interval by adjustments of the source-surface radius and the polar field correction. This is the model used for the calculation of Figure 2b. The Radial-2,5 model in Figure 3d is the same as that shown in Figures 3c and 3b (where it was labelled "WSO-Hoeksema").

In Figure 3d, the maximum latitudinal difference between one model and another is 16°, which is greater than the differences arising from the use of different sources of data or different source-surface distances. The Classic model clearly results in larger amplitude variations in the latitude of the HCS than do the other models. This difference arises because the radial boundary condition used in each of the three other models provides stronger polar fields than does the line-of-sight boundary condition used in the Classic model [*Wang and Sheeley, 1992].* This tendency for the Classic source-surface model to give larger variations in the amplitude of the HCS has been noted previously [e.g., *Crooker et al., 1997].*

For computational reasons, the MHD model of the interplanetary field must be based on a coarser grid at the inner boundary than is used for the source-surface models. As input to the MHD model, we therefore smoothed the NSO data to yield a grid 5° on a side. Figure 3e shows that the effect of the smoothing on the location of the HCS as calculated by the source-surface (SS-W&S) model is almost indiscernible. Finally, in Figure 3f, the HCS computed from the MHD model is compared to those calculated from the source-surface (SS-W&S) and the current-sheet (CS-W&S) models, all based on the same

smoothed input data. The MHD model is in closer agreement with the source-surface model than with the current-sheet model.

Figure 4 is a superposition of all the HCS locations calculated from eight of the models shown in Figure 3, with an exaggerated latitudinal scale. All models show an approximate double sinusoid, in agreement with the shape estimated by *Smith et al. [1995]* from analysis of Ulysses data. There is, however, uptoa210 spread in latitude for the HCS position calculated from the several models. The Classic model yields the steepest current sheet of the entire set, while the Radial-3.25 and the current-sheet models are the flattest,

Figure 5 shows the footpoints of open field lines computed from the SS-W&S source surface model (small blue dots) and from the MHD model (large red dots). The red dots are on a regularly spaced grid because those calculations started at the Sun to determine which grid points corresponded to open field lines. The blue dots are not regularly spaced, however, because their calculation started with a uniform distribution of open field lines at the source surface and then determined their origin at the Sun. The two models agree with each other remarkably well.

Figure 5 also shows the boundaries of coronal holes that can be observed in the He 10830 Å line as a result of the formation of this line being modulated by coronal radiation at wavelengths <504 Å [Goldberg, 1939; *Bohlin, 1977* and references therein; *Harvey,* 1996]. In He 10830 Å, coronal holes appear as brighter areas (less absorption due to less overlying coronal emission) at least 2-4 supergranules in size, with lower contrast of the network structure, and in areas of predominately unipolar magnetic fields. (Daily coronal hole maps are now available through the NSO/KP anonymous ftp archive at argo.tuc.noao.edu/kpvt/daily/lowres.) In Figure 5, solid boundaries denote coronal holes with positive magnetic polarity (field pointing outward from the Sun) while dashed lines denote negative or inward polarity.

The agreement of the model open field lines with the coronal hole boundaries is remarkably good; most open field lines originate in or near coronal holes and most of the coronal holes appear to produce open field lines. There are some noticeable disagreements, however:

1) The envelopes of the open field lines do not exactly trace the boundaries of the polar coronal holes; sometimes the open-field line regions are larger and sometimes they are smaller than the polar coronal hole. In some cases the details of the magnetic field in the photosphere offer a possible explanation for this mismatch. Consider the modeled open field between the main part of the south polar hole and its equatorward extension at longitudes of 180-240° in CR 1893. Although the models have the polarity of the field in that region being the same as that of the polar region (i.e., negative polarity), the photospheric magnetic field data show an extended area of opposite (positive) polarity between the polar hole and the poleward boundary of the extension. This area of opposite polarity may have been the cause of the break in the polar extension between rotations 1893 and 1894. Although there are two polarity inversions or neutral lines corresponding to closed fields between the polar extension and the polar hole, it may be that the open fields from the extension and from the polar hole merge above this area.

2) In other places where the open field lines originate equatorwards of the polar hole boundaries (e.g., the southern polar coronal hole at longitudes < -700), either the field lines originating outside the hole boundary really are open, or the models give misleading answers, because close examination of the solar data shows that those particular He 10830 Å boundaries cannot be enlarged.

3) At some longitudes (e.g., 3250-3600), the open field lines for the polar coronal holes calculated from the MHD model extend further equatorward than do the open field lines from the source-surface model. The MHD model uses the plasma density and temperature at the coronal base as boundary conditions (n_o = 4 x 10^8 cm^{-3} and TO = 1.8 x

10^6 K for this calculation). Values chosen for these quantities can influence the relative size of closed field regions and coronal hole boundaries; in other calculations we have found that decreasing the density will cause the coronal hole boundary to recede and the closed field region to expand. Thus a better agreement with the source-surface model might be achieved by using a smaller density in the MHD model.

4) In each rotation, the field lines apparently associated with the low-latitude hole near 130° longitude arise well to the north of the hole itself. Although there is no sign of a hole at the location of those open field lines, in CR 1893 the field to the north of the coronal hole was very weak. In each of the three rotations, there also are possible neutral-line crossings, where we expect the fields to be closed, at -30° N and longitudes of 90-100° in each of the three rotations.

5) There are also some coronal hole regions, such as the northern edge of the south polar coronal hole near longitudes of 170° and 300° and the two detached holes with northern polarity near 60° longitude, for which the models indicate that there are no open field lines. Examination of the open field lines calculated by the source-surface model using the high-resolution (rather than the smoothed) field data also show no open field lines from the two small northern coronal holes in CR 1893; so the lack of correlation between holes and open field lines is not an artifact of the smoothing procedure.

Despite these minor discrepancies, the general correlation of open-field footpoints with coronal holes suggests that the models can be used to identify the approximate locations of the source regions of the solar wind during this time.

Comparison of Models with Solar Wind Data

One method of comparing the spacecraft data to the solar data via the models is presented in Figure 6. This figure has six panels — one for each Barrington rotation for both Ulysses and WIND. The top panel of each frame shows the solar wind speed mapped back to the Sun on the basis of a radial, constant speed model. While this model may seem over-simplified, it does a remarkably good job because the effects of the solar wind coming up to speed is counterbalanced by the initial coronation of the plasma with the Sun. *Nolte and Roelof [* 1973] have argued that this method of mapping interplanetary features back to the Sun results in an error $\leq 10°$ in the longitude of the source region of the solar wind. Using a two-dimensional, single fluid MHD theory, *Pizzo [198* 1] has traced the evolution of a solar wind disturbance out from 0.3 AU to 1.0 AU, and then back in again to 0.3 AU, and then compared the longitudinal profiles of the solar wind parameters to those in the postulated initial disturbance. He found that the longitudinal extent and the location of the trailing edge of the disturbance was fairly well preserved and in good agreement with results obtained by constant-velocity mapping, but that irreversible processes led to strongly broadened and distorted profiles on the leading (highest longitude) edge of the disturbance. This effect can be seen in the profiles of mapped-back speeds shown in Figure 6; see for example, the high-speed stream centered near 180° longitude observed by WIND during CR 1893. The rising portion covers 60° of longitude, from 250° to 190°, while there is a steep drop, called a "dwell" by Nolte and Roelof, at -145° longitude. The heavier lines superimposed on the velocity profiles indicate probable intervals of transient flow from coronal mass ejections.

The bottom part of each frame in Figure 6 depicts(1) the outlines of the coronal holes, as also shown in Figure 5, and (2) red and blue lines, ending in dots or x's,

respectively, at the footpoints of the sources of the solar wind observed by Ulysses and WIND as calculated from the CS-W&S (red) and the SS-W&S (blue) models, based on NSO data. Mapped-back source and footpoint locations are given for each 5° in longitude along the spacecraft trajectory. The observed polarity of the interplanetary magnetic field (IMF) is indicated at the top of the bottom panels by a + or - sign for outward or inward fields, respectively, and the letter M for intervals of mixed polarity with multiple current sheet crossings. The mapped-back longitudes of the IMF polarity changes are indicated by dashed vertical lines. From Figure 6, we can make the following observations:

(1) At the higher latitudes sampled by Ulysses during CR 1892 and CR 1894 (i.e., more than -10° from the equator and away from the HCS), the IMF polarities predicted from the SS-W&S model and the CS-W&S model always agree with each other and the predicted polarity is correct 97% of the time.

(2) Dwells, crossings of the HCS, and the change in the footpoint region (from a polar to an equatorial hole, for example) often appeared at nearly the same mapped-back longitudes. Close inspection of Figure 6, however, reveals that at the lower latitudes the mapped-back locations of the HCS and the dwells were often at longitudes -20° less than the longitudes at which the models predicted changes in polarity. This finding is consistent with the observation by *Lepping et al. [1996]* that, for the period 1994/318 to 1995/093 (earlier than and overlapping the first part of the period studied in this paper), good correlations of the HCS data from WIND with the Classic or the Radial-3.25 models required an offset in the solar-wind propagation time between the source surface and 1 AU of approximately one day (on average, 1 day is equivalent to -13° of solar rotation, as seen from Earth). Lepping et al. attributed this additional travel time to the continuing acceleration of the solar wind outside of the source surface. The top section of Table 1 presents the percent of the model predictions that give the wrong polarity when compared to the mapped back observations of the lMF polarity. The middle section gives the number of degrees that each rotation's worth of data would have to be shifted to improve the agreement between the observations and the models; the average value of the required shift is 22°. The lower section provides the percent error taking an extra travel time equivalent to 22° rotation (1.7 days) into account and shows that this correction does improve the fit between the predicted and the observed crossings of the HCS. Table 1 also reveals that the current sheet (CS-W&S) model gives poorer results than the other models.

(3) Combination of the speed profiles (top panels of Figure 6), the locations of the observed HCS crossings (vertical dashed lines in the bottom panels), and the modeled source regions (bottom panels) with the estimated 22° systematic shift between the models and the mapped-back data allows us to identify the probable sources of the solar wind as a function of time or longitude. Such an analysis is presented in Table 2. In several

instances, one model indicated the source region as an equatorial coronal hole while the other model placed the source equatorward of one of the polar coronal hole boundaries. When the observed polarity of the IMF is opposite to that indicated by both models, the source is listed as "unknown". In Figure 7, the speeds of the different solar wind streams listed in Table 2 are grouped according to the probable type of source region. It can be seen from that Figure that the fast solar wind (>600 km/s) comes only from the polar coronal holes. (For most of those streams we have given only the peak speed without plotting the lower speeds encountered on the leading edges or the dwells.) Two of the streams which apparently originated in the polar coronal holes did not have speeds > 600 km/s; the models show the slower of those two streams originating quite close to, but nominally inside the hole boundary. Moderate- and low-speed streams emanate from equatorial coronal holes or from regions equatorward of the boundaries of the polar coronal holes. On average, the streams from the equatorial coronal holes are slightly faster than those from the regions close to the polar coronal holes. Slowest of all are the streams with "unknown" origin.

(4) At longitudes at which both spacecraft sampled flows from the same polar coronal hole, the one at the higher latitude saw a higher speed and the models showed the source region to be deeper into the hole. This effect is exhibited by both the Ulysses and WIND data at longitudes >300° in CR 1892 and at longitudes 140-190° in CR 1893. It is consistent with the general increase of solar wind speed toward the poles observed by Ulysses [e.g., *Phillips et al., 1995]*.

Latitude-Longitude Contours of Solar Wind Parameters

Because of the generally static condition of the Sun and solar wind during the five solar rotations of the Ulysses fast latitude scan, it is possible to examine the dependence of solar wind parameters on mapped-back longitude and latitude. Figure 8a shows contours

of the solar wind speed so derived. It is based on five rotations of Ulysses data plus CR 1893 data from WIND after removal of data believed to be associated with CMEs. The contours were calculated from hourly averages of solar wind speed which were averaged over 5° bins of mapped-back longitude and latitude based on the constant radial velocity assumption. Figure 8a reveals a curved band of low-speed wind ~50-60° wide (angular distance between the 700-km/s contours). The white asterisks in Figure 8 represent crossings of the HCS; broad intervals of multiple crossings have been represented by single asterisks at their midpoints. Qualitatively, the HCS encounters are confined to the central parts of the low-speed band, but, as previously pointed out by *Crooker at al. [1997],* at longitudes of 220-240°, the HCS was considerably southward of the region of minimum speed.

It is apparent that the latitudinal gradient of the solar wind speed is variable. This is illustrated in Figure 9, which shows cross plots of speed versus latitude at two different Barrington longitudes of 152 and 230°, selected to illustrate close to the extremes of latitude gradients. The principal gradients range from -14 to 28 km/sec-deg.

It is also quite apparent from Figure 8a that there is not a band of uniformly low speed along the HCS, which we assume is continuous across all longitudes. The minimum speed is close to 300 km/s at longitudes of 10-90°, but doesn't drop below 500 km/s near 145°. It is, however, quite likely that the speed contours have been distorted between the solar source and WIND or Ulysses; a speed minimum near 145° longitude may have been filled in by stream interactions. For this reason we next examine several properties of the solar wind that are believed to be conserved between the Sun and 1 AU. Figure 8b shows contours of the helium abundance n_α/n_p, binned as described above for the speed contours, but with the additional step of smoothing by a 5-bin running average along the Ulysses and

WIND trajectories. The lowest values of n_α/n_p generally trace out the HCS and coincide with the lowest speeds. The very low helium abundances at longitudes of 20-90° are consistent with the correlation between low helium abundance and the HCS reported by *Borrini et al. [1981],* but for longitudes >220°, the regions of lowest helium abundance do not coincide with observations of the HCS. When the HCS crossed longitudes of -140°, n_α/n_p apparently did not drop below 0.040.

Two other parameters that do not change with the propagation of the solar wind are the ionization temperature determined from the relative densities of O^{6+} and O^{7+} ions and the elemental composition of the wind, here represented by the ratio of the densities of Mg and O ions. These parameters were measured by the SWICS instrument on Ulysses, and were chosen for inclusion in this study because of their pronounced dependence on the solar wind type [*Geiss et al., 1995].* The contours shown in Figures 8c and 8d were calculated from three-hour averages binned into 5° of mapped-back latitude and longitude, and then smoothed by a 5-bin running average along the Ulysses trajectory. In general, these parameters show the same curved envelope as seen in Figure 8a with disconnected blotches of extreme values. The low-speed wind near 30° longitude apparently had an even lower ionization temperature and higher magnesium abundance than did the low speed wind from longitudes near 240°.

Discussion

In this paper we have taken advantage of the unique geometric situation during the Ulysses fast latitude scan when the Sun was quiet to gain new insights into latitude and longitude variations of the solar wind near solar-activity minimum. During this period, the

HCS and plasma parameters varied with longitude as a double sinusoid to yield a 4-sector structure at low latitudes.

We compared several different source-surface models of the interplanetary magnetic field with each other and with a 3-dimensional MHD model, Our intent was not to perform an exhaustive study of the effectiveness of different IMF models, but rather to understand the magnitude of the differences appropriate to the particular solar configuration in early 1995 to aid in interpretation of the Ulysses fast-scan data. Each of the models tested resulted in the observed double sinusoidal structure of the IMF. Like others before us, we found variations of up to -20° in the latitude of the HCS using different models, but model differences that depended on the choice of the source of data, from the Wilcox Solar Observatory or from the National Solar Observatory/Kitt Peak, were much smaller, < -10°. The Stanford Classic model yielded the largest amplitude variations of the HCS, while the Stanford Radial-3.25 and the current sheet models gave the flattest HCS. For this particular time, the results of the current sheet model were in poorer agreement with the observations than were the other models. The results of the MHD model were in better agreement with the source-surface model without a current sheet than with the current-sheet model. The reason for this result is not clear to us. It would be interesting to see if this also holds at other times.

When we compared the predictions of the HCS locations to the observations by Ulysses and WIND by mapping the data back to the source surface with a constant radial velocity approximation, we found that a best fit was obtained by adding an extra travel time equal to 22° of solar rotation (1.7 days). This result agrees with the preliminary findings of *Lepping et al. [1995].* It disagrees with the results of *Ho et al. [* 1997] who reported a very large discrepancy of 75-95° for WIND and 80-110° for Ulysses; Ho et al. did not describe how they obtained that particular result. An additional travel time of a day or two does not

invalidate the usefulness of the constant radial flow approximation for mapping solar wind features back to the photosphere, however. At a source surface at 2.5 or 3.25 R_s, the solar wind is probably still accelerating, but much of the corotational velocity has probably already been lost. If the mapping process is stopped at the source surface, the full cancellation of the corotational and acceleration effects noted by *Nolte and Roe/of [* 197 3] is not yet achieved. The Helios observations showed that the slow solar wind continues to accelerate over the range 0.3 to 1.0 AU while the fast wind decelerates [*Schwenn* et *al.*, 1981]. Future analyses should perhaps include the solar wind speed as a parameter in comparing source surface and interplanetary fields.

We also compared the source of open field lines calculated by a source-surface model and the MHD model to the locations of coronal holes observed in the He 10830 Å line. Qualitatively, there was a good match for both models, but some differences were found in the details. There was often not a very close match between the boundaries of the coronal holes and the envelope of the open field lines. In some places, the open field lines extended beyond the coronal hole boundaries and elsewhere there appeared to be closed-field regions just inside the boundaries. Because the same mismatch of patterns persisted through all three rotations, one cannot invoke time variations as an explanation.

When the solar wind speeds observed by WIND and Ulysses are compared to the source regions computed from the models, it is found that the fastest wind came from the polar coronal holes. The deeper into the polar hole a footpoint was, the faster the wind. Some of the moderate- or low-speed streams appeared to come from smaller coronal holes at lower latitudes, a result which is consistent with earlier conclusions that the speed of the solar wind scales with the coronal hole area [*Nolte et al.*, 1976]. The models suggest that regions of open field lines just equatorwards of the polar coronal hole boundaries are additional sources of moderate- or low-speed wind,

Both the postulated sources of low-speed wind, i.e., the low-latitude coronal holes and the fringes of the polar coronal holes, are regions of greater than average areal

expansion of magnetic flux tubes near the Sun. The inverse correlation of solar wind speed and near-Sun flux-tube divergence rate [Levine *et al.*, 1977; *Wang and Sheeley, 1990]* is now well established. Figure 10 shows contours of the expansion factor calculated from the SS-W&S model averaged over the three Barrington rotations 1892-1894. Comparison of Figures 10 and 8a illustrates this inverse correlation.

What about the four low-speed streams of "unknown" origin (Figure 7) and the one low-speed stream that appears to originate in the north polar coronal hole (Table 2 and Figure 7)? The most likely explanation is the fallibility of the models in source identification, especially near the HCS. We saw from Figure 4 that the location of the HCS can vary by up to 20° from one model to another. The four streams of unknown origin might have identifiable sources on the basis of some model other than the two used in the construction of Figure 6. An alternative explanation of the "problem" streams is that they originated in regions where the field was temporarily open for times short compared to the 27-days required to construct the synoptic field maps on which the models are based. These streams did not, however, show any of the common signatures of CMEs. There may also be small regions of open field lines, some possibly originating in active regions, that are not picked up by modeling of the low-resolution magnetograph data.

Contour diagrams of the latitude and longitude variations of several solar wind parameters reveal that there is a general correlation of the heliospheric current sheet with a band of low speed, low helium abundance , high ionization temperature and high ratio of the magnesium to oxygen ratio (i.e., enhanced overabundance of an element with a low first ionization potential). These findings are in agreement with many earlier reports. We found, however, that the plasma properties are very nonuniform along the inferred location of the current sheet. Thus there is no unique dependence of any plasma parameter, such as speed, on magnetic latitude, in agreement with a recent conclusion by *Wang et al. [*1997].

Our contour maps show heliographic latitude gradients of the solar wind speed ranging from 14 to 28 km/s/deg. These results are consistent with earlier studies based on superposed epoch analyses [*Zhao and Hundhausen*, 1981] or on yearly averages of interplanetary scintillation data near solar activity minimum [*Rickett and Coles*, 1991]. We saw no evidence for the very steep 30 to 100 km/s/deg gradients inferred by *Schwenn et al. [1978]* from Helios data nor for the 47 km/s/deg gradient reported by *Ho et al. [1997]* from the same set of WIND and Ulysses data analyzed in the present paper. The latitudinal resolution (i.e., the change in latitude per solar rotation) of the Ulysses data is -22°, which limits the detection of any steep latitudinal gradients that maybe present except for CR 1893 when Ulysses crossed the latitude of the WIND trajectory,. It should also be noted that the averaging inherent in the construction of Figure 8 may lead to smoothing of steep gradients in the solar wind speed.

With the Ulysses measurement rate of one solar wind spectrum every 4 or 8 minutes, the angular resolution in longitude **can be extremely fine. Steep longitudinal** gradients often occur in the dwells found at the trailing edges of high-speed streams in mapped-back data. Some dwells suggest extremely sharp longitudinal gradients, which could be interpreted as gradients in magnetic latitude if the HCS is highly inclined to the equator. Examples of steep dwells are prominent near 300° longitude during CR 1892 and near 125° longitude in CR 1894 in the WIND data in Figure 6. Are dwells real? Do they indicate that there really are extremely steep gradients in the source regions of the solar wind? The contour diagram in Figure 8a suggests that this is not the case, that major changes in the solar wind regime occur over tens of degrees. Another argument in support of the steepness of dwells being some sort of an artifact comes from the work of *Pizzo* [1981]; when he used an MHD model to map a gradient of -50 km/s/deg from 0.3 AU out to 1 AU and then back to 0.3 AU again, the trailing edge profile, while centered at the same

longitude as the original gradient, developed a reversed or overhanging structure, much more pronounced than that shown in the WIND data near 300° longitude in CR 1892. Further research into the cause of the dwells might be very fruitful.

Acknowledgments. This paper presents the results of research performed at the Jet Propulsion Laboratory of the California Institute of Technology under contract to the National Aeronautics and Space Administration (NASA). The work was initiated and partly carried out at the International Space Science Institute, Bern, Switzerland, as part of a joint IACG/ISSI Working Group Project on "Open and Closed Fields and the Solar Wind" supported by 1SS1. The work by ABG, KLH, JTH, AJL, RPL, JTS and Y-MW is supported by NASA. JAL and ZM received support from NASA and NSF. The NSO/Kitt Peak data used here are produced cooperatively by NSF/NOAO, NASA/GSFC, and NOAA/SEC.

References

Balogh, A., T. J. Beek, R. J. Forsyth, P. C. Hedgecock, R. J. Marquedant, E. J. Smith, D. J. Southwood, and B. T. Tsurutani, The magnetic field investigation on the Ulysses mission: Instrumentation and preliminary scientific results, *Astron. Astrophys. Suppl.*, 92, 221, 1992.

Bame, S. J., D. J. McComas, B. L. Barraclough, J. L. Phillips, K. J. Sofaly, J. C. Chavez, B. E. Goldstein, and R. K. Sakurai, The Ulysses solar wind plasma experiment, *Astron. and Astrophys. Suppl., 92, 237, 1992.*

Bohlin, J. D., An observational definition of coronal holes, in *Coronal Holes and High Speed Wind Streams*, edited by J. B. Zirker, p. 27, Colorado Assoc. Univ. Press, Boulder, CO, 1977.

Borrini, G., J. T. Gosling, S. J. Bame, W. C. Feldman, and J. M. Wilcox, Solar wind helium and hydrogen structure near the heliospheric current sheet: a signal of coronal streamers at 1 AU, *J. Geophys. Res.*, 86, 4565, 1981.

Crooker, N. U., A. J. Lazarus, J. L. Phillips, J. T. Steinberg, A. Szabo, R. P. Lepping, and E. J. Smith, Coronal streamer belt asymmetries and seasonal solar wind variations deduced from Wind and Ulysses data, *J. Geophys. Res.*, 102,4673, 1997.

Geiss, J. et al., The southern high-speed stream: results from the S WICS instrument on Ulysses, *Science*, 268, 1033, 1995.

Gloeckler, G. L., et al., The solar wind ion composition spectrometer, *Astron. Astrophys. Suppl.*, *92, 267*, 1992.

Goldberg, L., The temperature of the solar chromosphere, *Astrophys. J.*, 89,673, 1939.

Harvey, K. L., Coronal structures deduced from photospheric magnetic field and He I λ10830 observations, in *Solar Wind Eight*, edited by D. Winterhalter, J. T. Gosling, S,. R. Habbal, W. S. Kurth, and M. Neugebauer, p. 9, Am. Inst. of Phys., Woodbury, N. Y., 1996.

Ho, C. M., B. T. Tsurutani, J. K. Arballo, B. E. Goldstein, R. P. Lepping, K. W. Ogilvie, A. J. Lazarus, and J. T. Steinberg, Latitudinal structure of the heliospheric current sheet and corotating streams measured by WIND and ULYSSES, *Geophys. Res, Left.*, 24,915, 1997.

Hoeksema, J. T., J. M. Wilcox, and P. H. Schemer, The structure of the heliospheric current sheet: 1978-1982, *J. Geophys. Res.*, 88, 9910, 1983.

Lepping, R. P., et al., The WIND magnetic field investigation, *Space Sci. Rev., 71*, 207, 1995.

Lepping, R. P., A. Szabo, M. Peredo, and J. T. Hoekserna, Large-scale properties and solar connection of the heliospheric current and plasma sheets: WIN]> observations, *Geophys. Res. Lett.*, 23, 1199, 1996.

Levine, R. H., M. D. Altschuler, and J. W. Harvey, Solar sources of the interplanetary magnetic field and solar wind, *J. Geophys. Res.*, 82, 1061, 1977.

Linker, J. A., and Z. Mikic, Extending coronal models to Earth orbit, in *Coronal Mass Ejections*, edited by N. Crooker, J. Jocelyn, and J. Feynrnan, p. 269, AGU, Washington, D. C., 1997.

Linker, J. A., Z. Mikic, and D. D. Schnack, Global coronal modeling and space weather prediction, in edited by K. S. Balasubramanian et al., p. 208, Astron. Sot. of Pacific, 1996.

Mikic, Z., and J. A. Linker, The large-scale structure of the solar corona and inner heliosphere, in *Solar Wind Eight, AIP Proc. 382,* edited b y D. Winterhalter et al,, p. 104, Amer. Inst. Phys., Woodbury, N. Y., 1996.

Nolte, J. T., and E. C. Roelof, Large-scale structure of the interplanetary medium. 1: High coronal source longitude of the quiet-time solar wind, *Solar Phys.*, 33, 241, 1973.

Nolte, J. T., A. S. Krieger, A. F, Timothy, R. E. Gold, E. C. Roelof, G. Vaiana, A, J. Lazarus, J. D. Sullivan, and P. S. McIntosh, Coronal holes as sources of solar wind, *Solar Phys.*, 46,303, 1976.

Ogilvie, K, W., et al., SWE: A comprehensive plasma instrument for the WIND spacecraft, The Global Geospace Mission, *Space Sci. Rev., 71, 55, 1995.*

Phillips, J. L., et al,, Ul ysses solar wind plasma observations from pole to pole, *Geophys. Res. Lett.*, 22,3301, 1995,

Pizzo, V. J., On the application of numerical models to the inverse mapping of solar wind flow structures, *J. Geophys. Res.*, 86,6685, 1981.

Rickett, B. J., and W. A. Coles, Evolution of the solar wind structure over a solar cycle: Interplanetary scintillation velocity measurements compared with coronal observations, *J. Geophys. Res.*, 96, 1717, 1991.

Schatten, K., J. W. Wilcox, and N. F. Ness, A model of the interplanetary and coronal magnetic fields, *Solar Phys., 6, 442, 1969.*

Schatten, K. H., Current sheet model for the solar corona, Cosmic *Electrodynamics,* 2, 232, 1971.

Schwenn, R., M. D. Montgomery, H. Rosenbauer, H. Miggenrieder, K.-H. Mühlhäuser, S. J. Bame, W. C. Feldman, and R. T. Hansen, Direct observations of the latitudinal extent of a high speed stream in the solar wind, *J. Geophys. Res.*, 83, 1011, 1978.

Schwenn, R., K.-H. Mühlhäuser, E. Marsch, and H. Rosenbauer, Two states of the solar wind at the time of the solar activity minimum II. Radial gradients of plasma parameters in fast and slow streams, in *Solar Wind Four*, edited by H. Rosenbauer, p. 126, Max-Planck-Institut, Katlenburg-Lindau, Germany, 1981.

Smith, E. J., and R. G. Marsden, Ulysses Observations from pole-to-pole: An introduction, *Geophys. Res. Lett.*, 22, 3297, 1995.

Smith, E. J., A. Balogh, M. E. Burton, G. Erdos, and R. J. Forsyth, Results of the Ulysses fast latitude scan: Magnetic field observations, *Geophys. Res. Lett.*, 22, 3325, 1995.

Wang, Y.-M., Nonradial coronal streamers, *Astrophys. J.*, -/56, L119, 1996.

Wang, Y.-M. and N. R. Sheeley, Jr., Solar wind speed and coronal flux-tube expansion, *Astrophys. J., 355,726,* 1990.

Wang, Y.-M., and N. R. Sheeley, Jr., On potential field models of the solar corona, *Astrophys. J., 392, 310, 1992.*

Wang, Y.-M., and N. R, Sheeley, Jr., Solar implications of Ulysses interplanetary field measurements, *Astrophys. J., 447, L143, 1995.*

Wang, Y.-M., N. R. Sheeley, Jr., J. L. Phillips and B. E. Goldstein, Solar wind stream interactions and the wind speed-expansion factor relationship, *Astrophy. J., submitted, 1997.*

Zhao, X., and J. T. Hoeksema, Prediction of the interplanetary magnetic field strength, *J. Geophys. Res., 100,* 19, 1995.

Zhao, X.-P., and A. J. Hundhausen, Organization of solar wind plasma properties in a tilted, heliomagnetic coordinate system, *J. Geophys. Res.,* 86,5423, 1981.

Table 1. Comparison of mapped-back longitudes of observed low-latitude HCS crossings with longitudes predicted by models. The source of the data are indicated as National Solar Observatory/Kitt Peak (NSO) or Wilcox Solar Observatory (WSO). See text for definition of models.

(a) % wrong polaxity (based on constant velocity map-back)

SIC: CR	MHD (NSO)	SS-W&S (NSO)	CS-W&S (NSO)	Classic (WSO)	Radial-3.25 (wSo)
U:1893	19	11	21		
W: 1892	21	22	21	19	16
W:1893	26	26	26		
W:1894	29	26	33		
Average	24	21	25	19	16

(b) Degrees longitudinal shift between mapped-back observed HCS (or middle of "mixed" polarity interval) and model HCS:

S/C: CR	MHD (NSO)	SS-W&S (NSO)	CS-W&S (NSO)	Classic (WSO)	Radial-3.25 (WSO)
W:1892	26	27	32	21	20
W:1893	28	29	26		
W:1894	33	32	21		
Average	25	24	22	21	20

(c) % wrong polarity after shift of 22°:

S/C: CR	MHD (NSO)	SS-W&S (NSO)	CS-W&S (NSO)	Classic (WSO)	Radial-3.25 (wSo)
W:1892	4	7	15	4	4
W:1893	6	6	15		
W:1894	18	8	28		
Average	12	9	22	4	4

Table 2. Summary of solar wind streams shown in Figure 6. Parameters are the spacecraft and Barrington rotations, the mapped back longitude of the solar wind, the range of speeds in the stream, and the probable source as derived from the models.

S/C: CR	Longitude	Speed	Source
U:1892	360-155	≤780	SCH
U:1892	155-140	580-820	CME
U:1892	140-95	500-580	SCH
U:1892	95-40	340-460	equatorward of SCH
U:1892	40-0	320-440	ECH or equatorward of SCH
U:1893	360-300	≤710	SCH
U:1893	300-250	350-520	ECH
U:1893	250-150	≤610	SCH extension
U:1893	150-100	400-590	ECH
U:1893	100-45	390-500	equatorward of NCH
U:1893	45-1o	330-360	ECH
U:1893/4	10-240	325-550	ECH or equatorward of NCH
U:1894	240-195	325-430	NCH (near boundary)
U:1894	195-165	410-430	unknown
U:1894	165-0	≤750	NCH
W:1892	360-290	≤720	SCH
W:1892	290-235	325-480	CME and EQH
W:1892	235-135	≤680	SCH
W:1892	135-100	390-460	ECH
W:1892	100-70	290-350	equatorward of NCH
W:1892	70-40	260-290	unknown
W:1892/3	40-340	300-510	ECH
W:1893	340-300	≤690	SCH
W:1893	300-240	380-475	ECH
W:1893	240-140	≤760	SCH
W:1893	140-90	340-430	ECH
W:1893	90-70	290-310	equatorward of NCH
W:1893	70-40	290-340	CME
W:1893/4	40-340	300-520	ECH
W:1894	340-315	410-550	ECH or equatorward of SCH
W:1894	315-280	350-430	ECH
W:1894	280-250	250-340	CME
W:1894	250-230	320-370	unknown
W:1894	230-125	≤710	SCH
W:1894	125-70	325-375	equatorward of NCH
W:1894	70-50	325-375	equatorward of SCH
W:1894	50-25	300-330	unknown
W:1894	25-O	330-440	ECH

U: Ulysses
W: WIND
ECH: Equatorial coronal hole
NCH: North polar coronal hole
SCH: South polar coronal hole or its extension

Figure Captions

Figure 1. Heliographic latitude and longitude of mapped-back source regions of the solar wind observed by Ulysses during Barrington Rotations (CR) 1891-1895 and by WIND during CR 1892-4 calculated from the spacecraft locations and the observed speeds assuming radial flow at constant speed between the Sun and the spacecraft.

Figure 2. (a) Solar wind speed observed at WIND during three 27-day rotations. The heavy symbols denote probable intervals of transient flow from coronal mass ejections. (b) Heliographic latitude and longitude of the heliospheric current sheet for five Carrington rotations as calculated by the "Classic" method (see text).

Figure 3. Comparisons of heliospheric current sheet locations during Barrington rotation 1892 as calculated using the different models described in the text.

Figure 4. Superposition of eight different models of the location of the heliospheric current sheet during Barrington rotation 1892. Note that the latitudinal scale is exaggerated compared to the longitudinal scale.

Figure 5. (Lines) boundaries of coronal holes as observed in the He 10830 Å spectral line. The boundaries of coronal holes with outward (positive) magnetic polarity are drown as solid lines, while dashed lines denote inward (negative) polarity. (Dots) Computed footpoints of magnetic field lines open to the solar wind as computed by the MHD (large red dots) and source-surface (small blue dots) models.

Figure 6. (Top panels) Mapped-back solar wind speed versus longitude, where the heavy lines denote intervals of transient flow from CMEs. (Bottom panels) Lines extending from the mapped-back spacecraft latitude and longitude to the footpoints or source regions of the solar wind as computed from the CS-W&S (red lines with dots) and the SS-W&S (blue lines with x's) models. See text for definition of models. The lines are superimposed on the coronal hole boundaries as in Figure 5. The polarities of the interplanetary magnetic field observed by Ulysses and WIND are indicated by the symbols +, -, or M for outward, inward, and mixed polarities, respectively, with dashed vertical lines denoting the mapped-back longitudes at which the changes in polarity occurred,

Figure 7. Distribution of speeds from different sources of the solar wind as deduced from Figure 6 and Table 1. The different types of sources are grouped, using the notation PCH = polar coronal hole and ECH = equatorial coronal hole.

Figure 8. (a) Contours of solar wind speed. The white areas denote speeds >750 km/s. Note that the latitude scale is exaggerated. The white asterisks indicate locations of HCS crossings. The contours are calculated from averages over 5°x50 bins in latitude and longitude from 5 rotations of Ulysses data and for WIND data for CR 1893. (b) Contours of the alpha-particle abundance n_α/n_p computed from running 5-bin averages along the spacecraft trajectories. (c) Contours of the ionization temperature calculated from the density ratio of O^{7+} to O^{6+} ions, in units of 10^6 K, computed from running 5-bin averages along the spacecraft trajectories. (d) Contours of the density ratios of Mg to O computed from running 5-bin averages along the spacecraft trajectories.

Figure 9. Speed versus latitude at Carrington longitudes of 152° and 230°. These are cross plots of selected data in Figure 8a.

Figure 10. Contours of the solar wind expansion factor calculated from the source-surface model, in the same format as Figure 8a. The data in each 5°x50 bin were averaged over Carrington rotations 1892 through 1894.

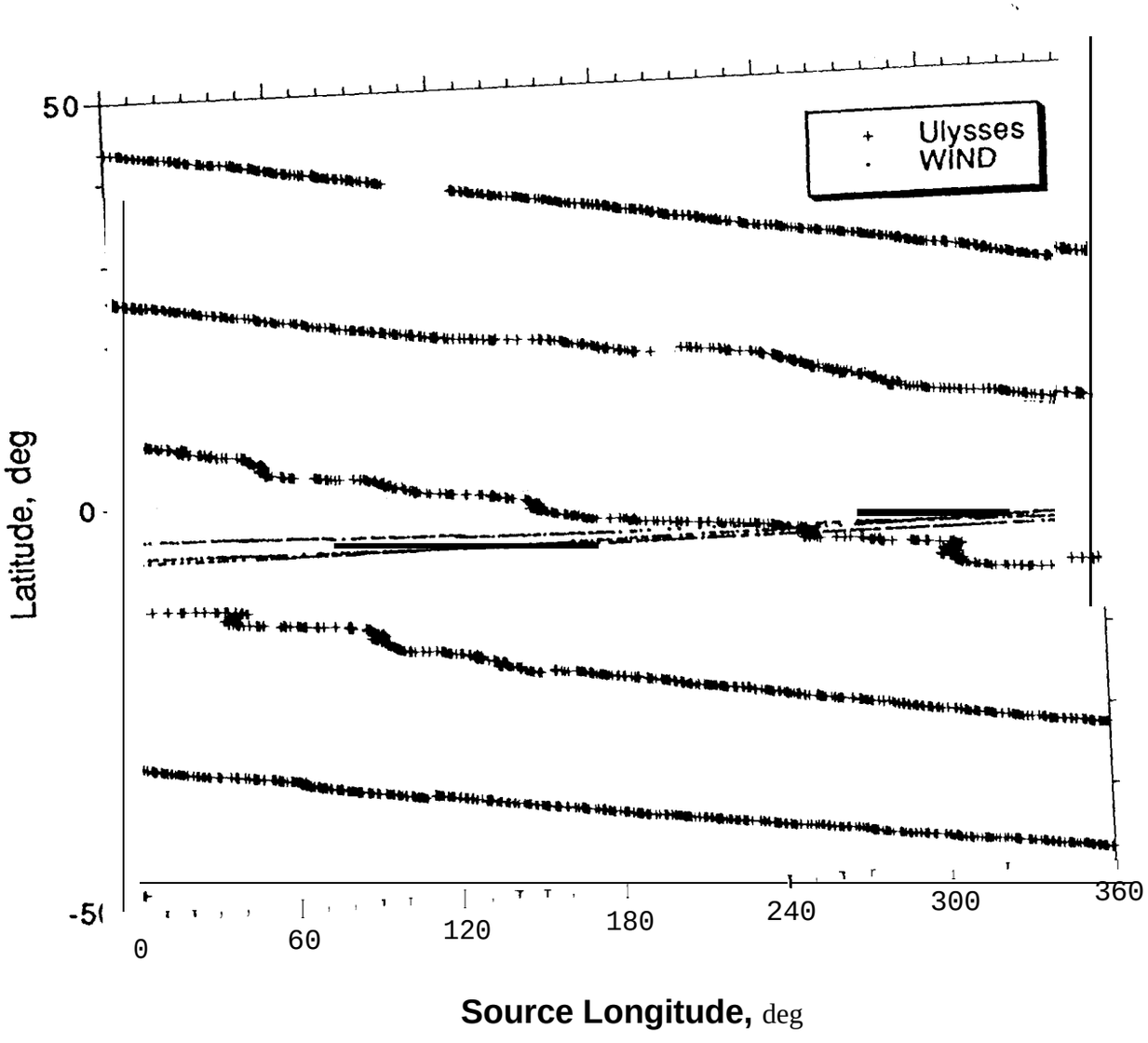
Ulysses
WIND
50
0
-5(
Latitude, deg
0
60
120
180
240
300
360
Source Longitude, deg

Fig 1

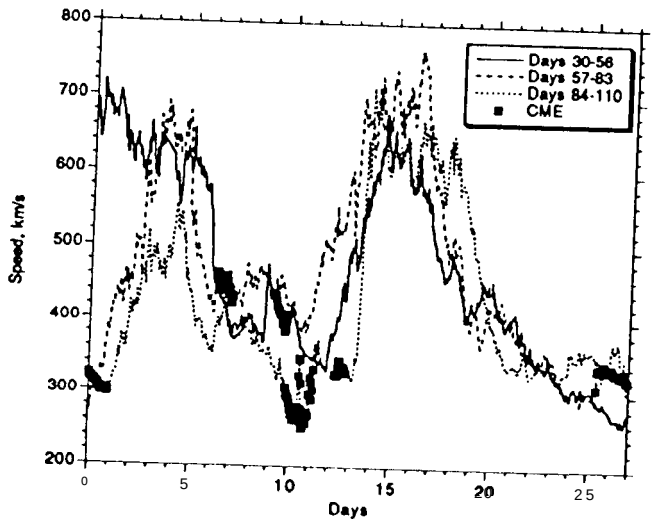
800
700
600
500
400
300
200
Speed, km/s
0
5
10
15
20
25
Days
Days 30-56
Days 57-83
Days 84-110
CME

Fig 2a

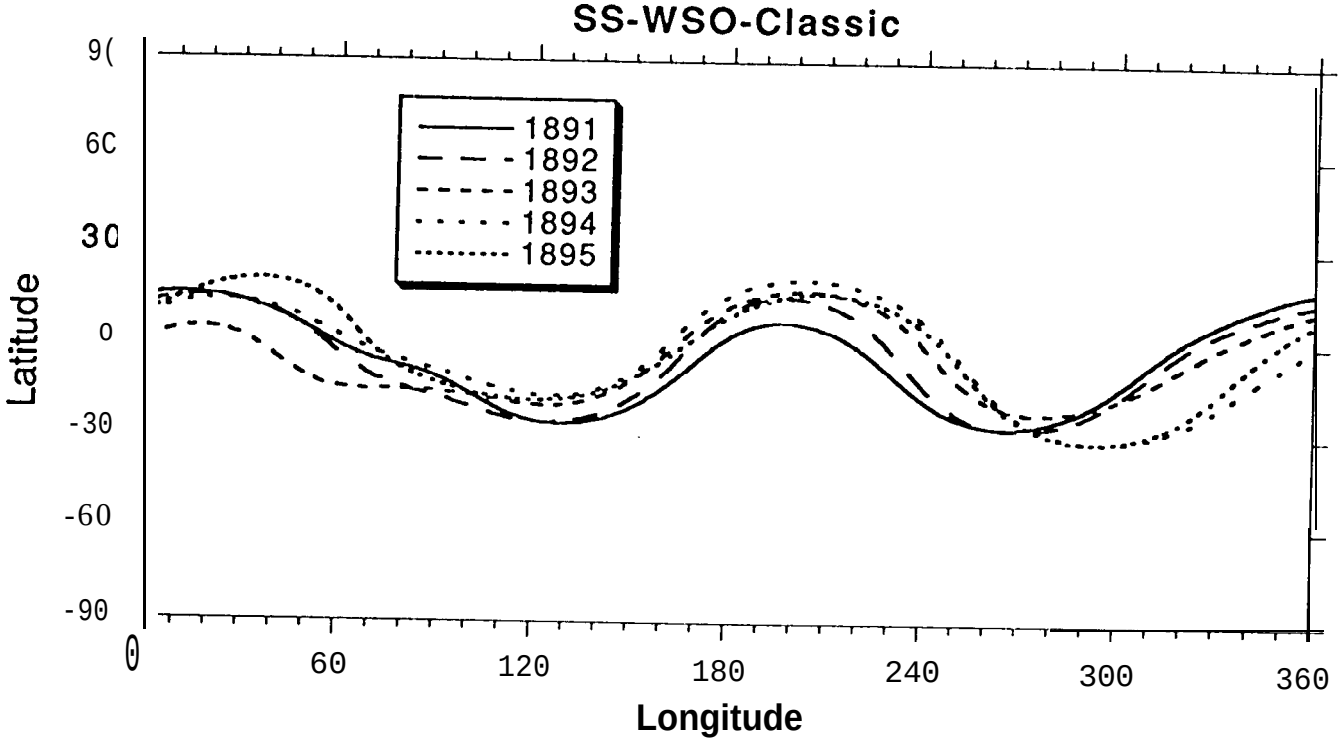
SS-WSO-Classic
1891
1892
1893
1894
1895
Latitude
9(
6C
30
0
-30
-60
-90
0
60
120
180
240
300
360
Longitude

Fig 2b

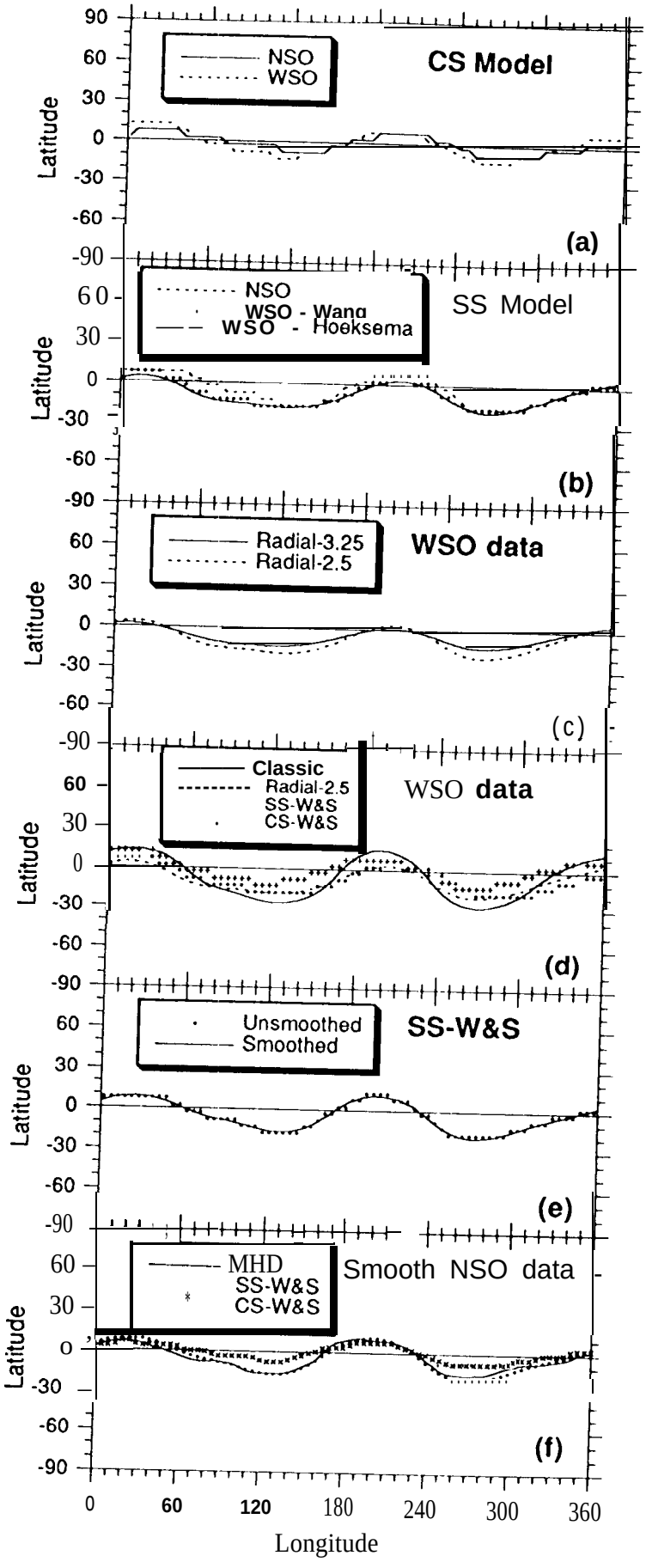
NSO
WSO
CS Model
(a)
NSO
WSO - Wang
WSO - Hoeksema
SS Model
(b)
Radial-3.25
Radial-2.5
WSO data
(c)
Classic
Radial-2.5
SS-W&S
CS-W&S
WSO data
(d)
Unsmoothed
Smoothed
SS-W&S
(e)
MHD
SS-W&S
CS-W&S
Smooth NSO data
(f)
Latitude
Longitude
90
60
30
0
-30
-60
-90
0
60
120
180
240
300
360

Fig 3

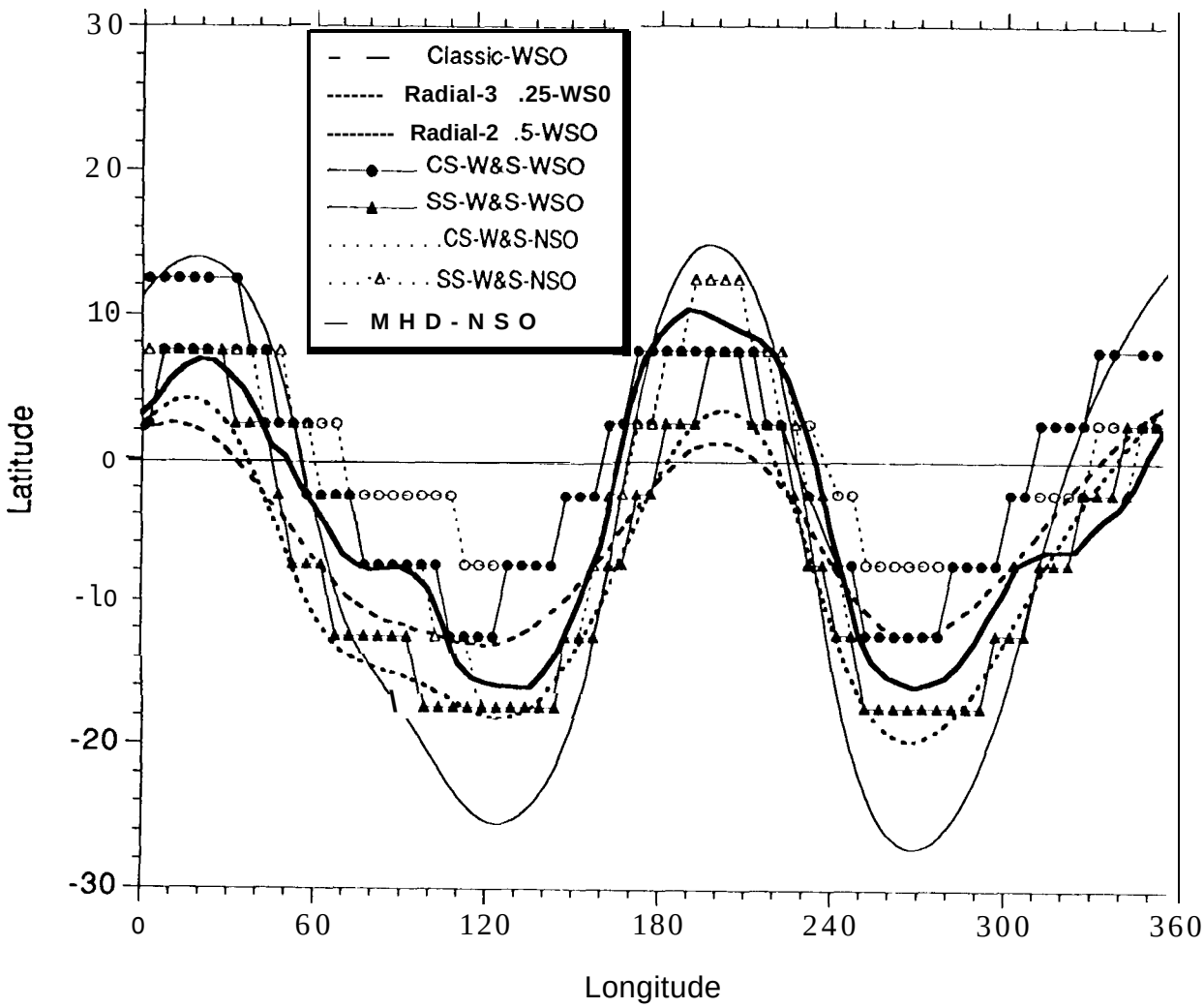
30
20
10
0
-lo
-20
-30
Latitude
0
60
120
180
240
300
360
Longitude
Classic-WSO
Radial-3 .25-WS0
Radial-2 .5-WSO
CS-W&S-WSO
SS-W&S-WSO
CS-W&S-NSO
SS-W&S-NSO
M H D - N S O

Fig. 4

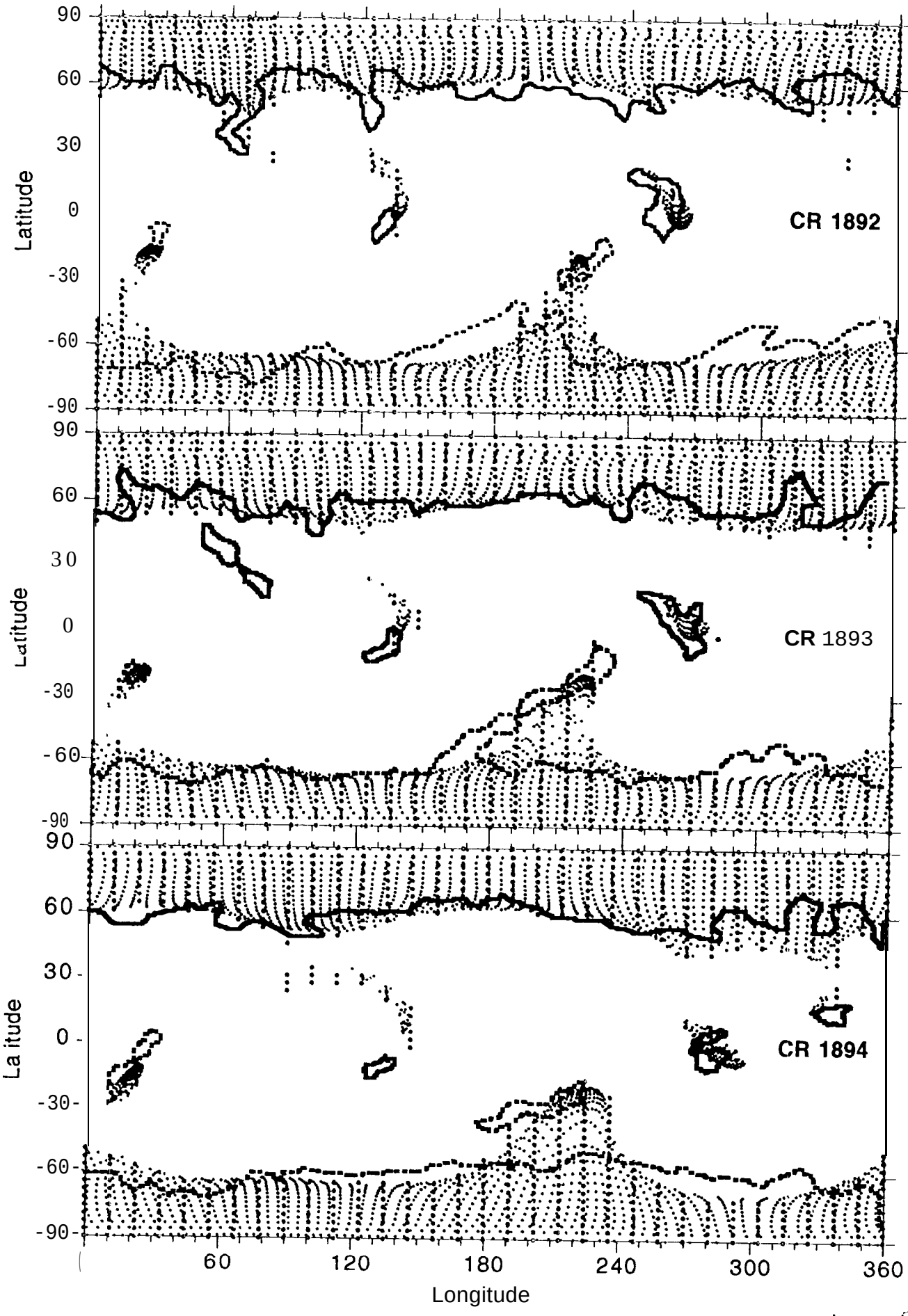
90
60
30
0
-30
-60
-90
Latitude
CR 1892
90
60
30
0
-30
-60
-90
Latitude
CR 1893
90
60
30
0
-30
-60
-90
La itude
CR 1894
60
120
180
240
300
360
Longitude

Fig 5

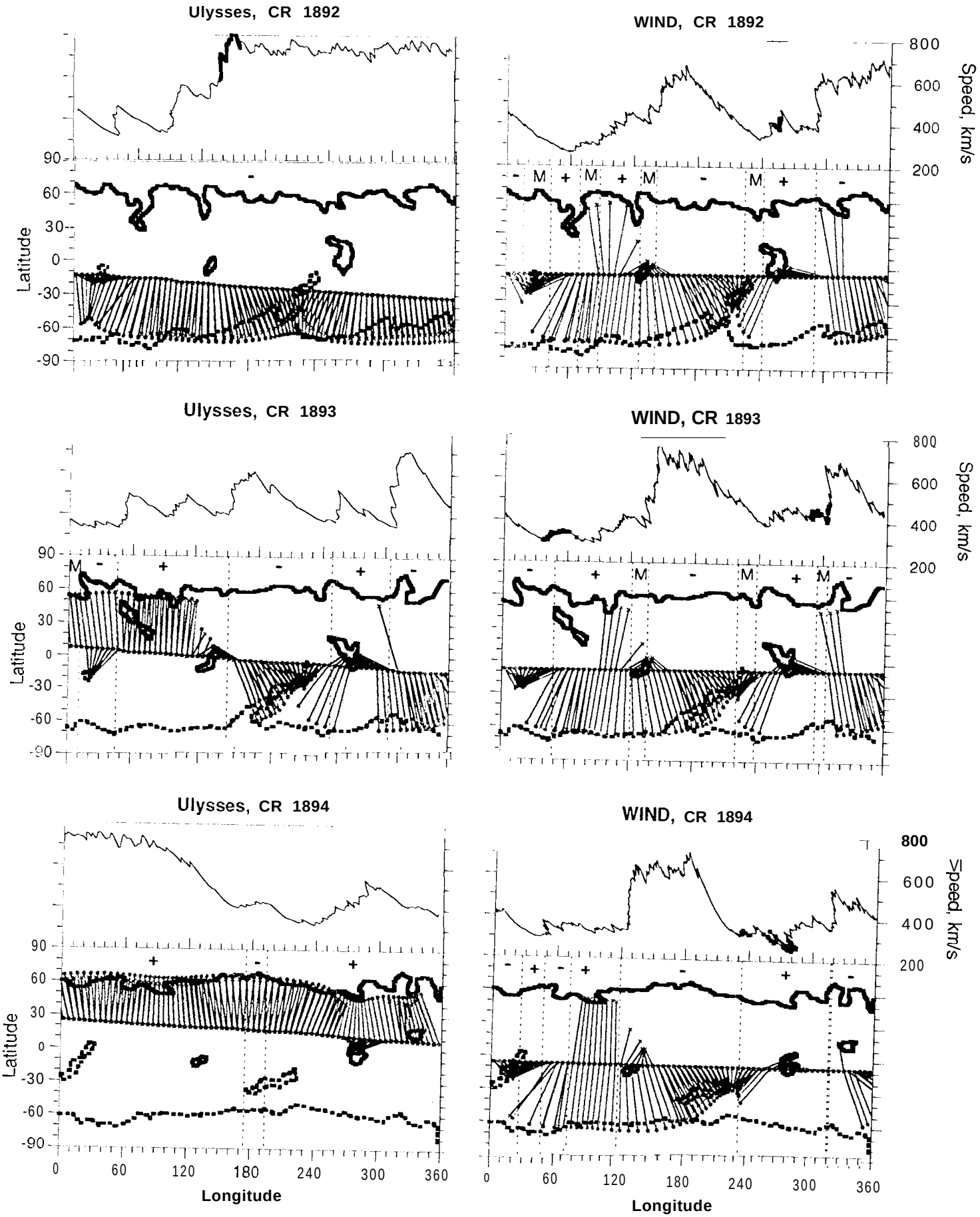
Ulysses, CR 1892
WIND, CR 1892
Ulysses, CR 1893
WIND, CR 1893
Ulysses, CR 1894
WIND, CR 1894
Latitude
Longitude
Speed, km/s
90
60
30
0
-30
-60
-90
0
60
120
180
240
300
360
800
600
400
200
M
+
-

Fig. 6

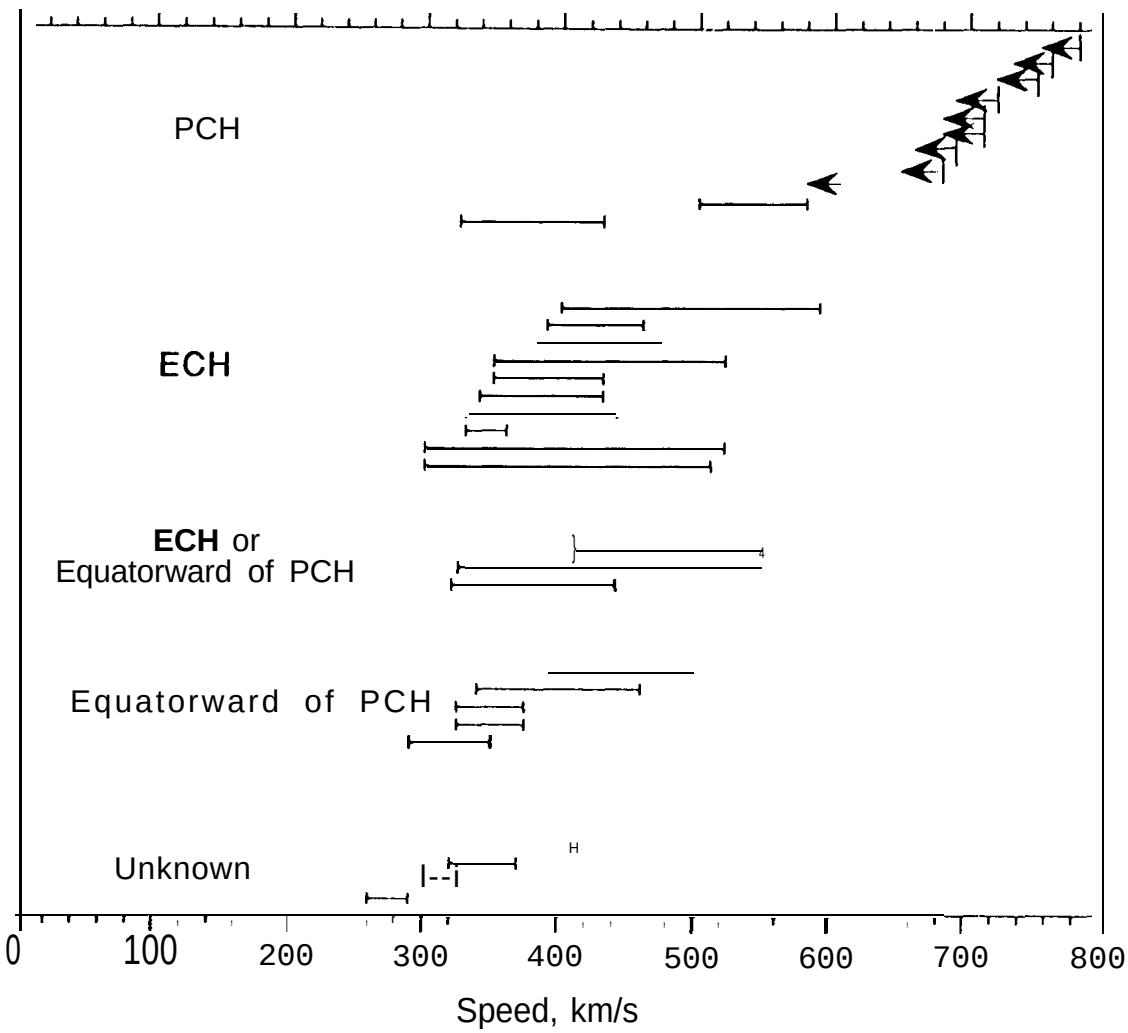
PCH
ECH
ECH or
Equatorward of PCH
Equatorward of PCH
Unknown
0
100
200
300
400
500
600
700
800
Speed, km/s

Fig 7

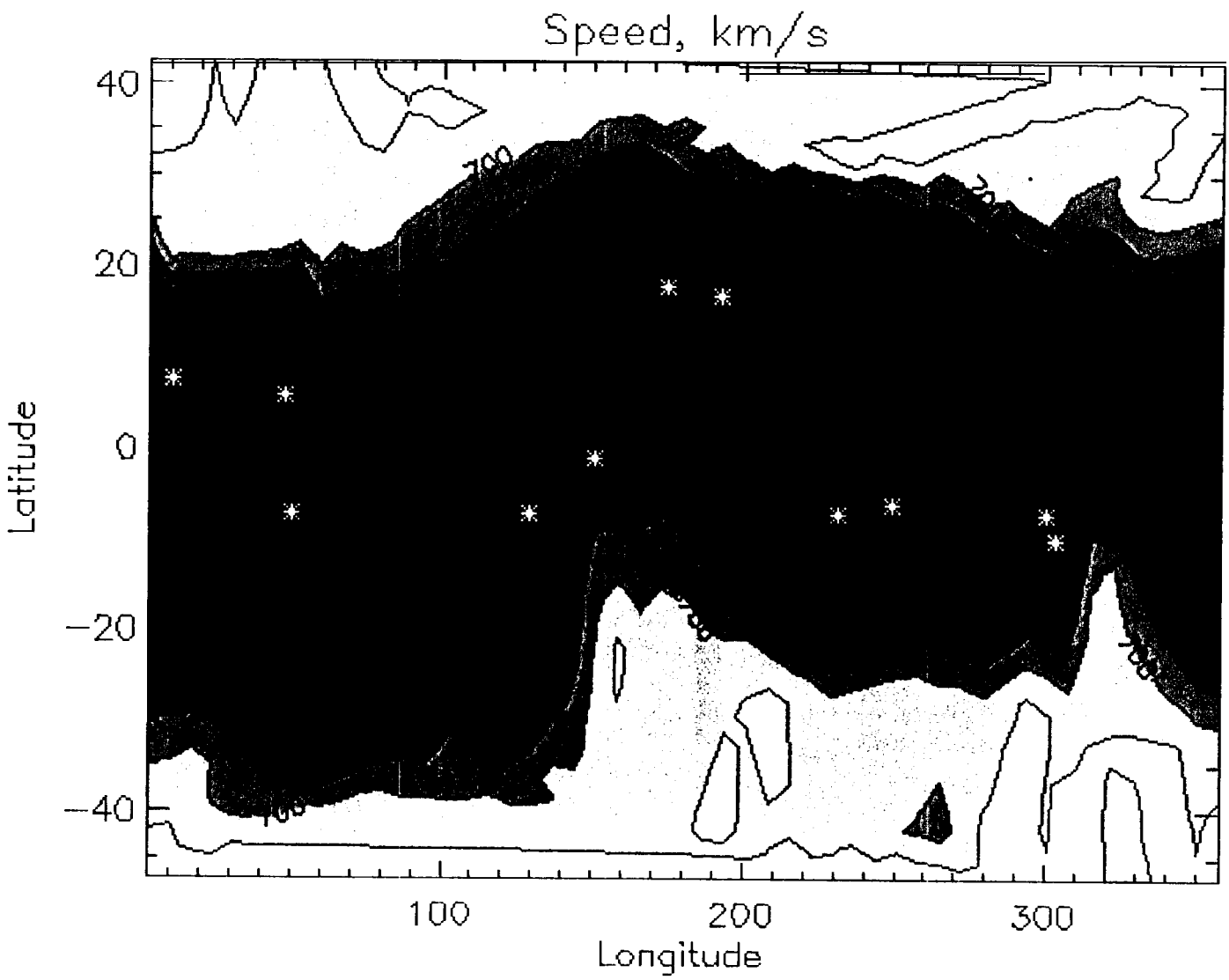

Fig 8a

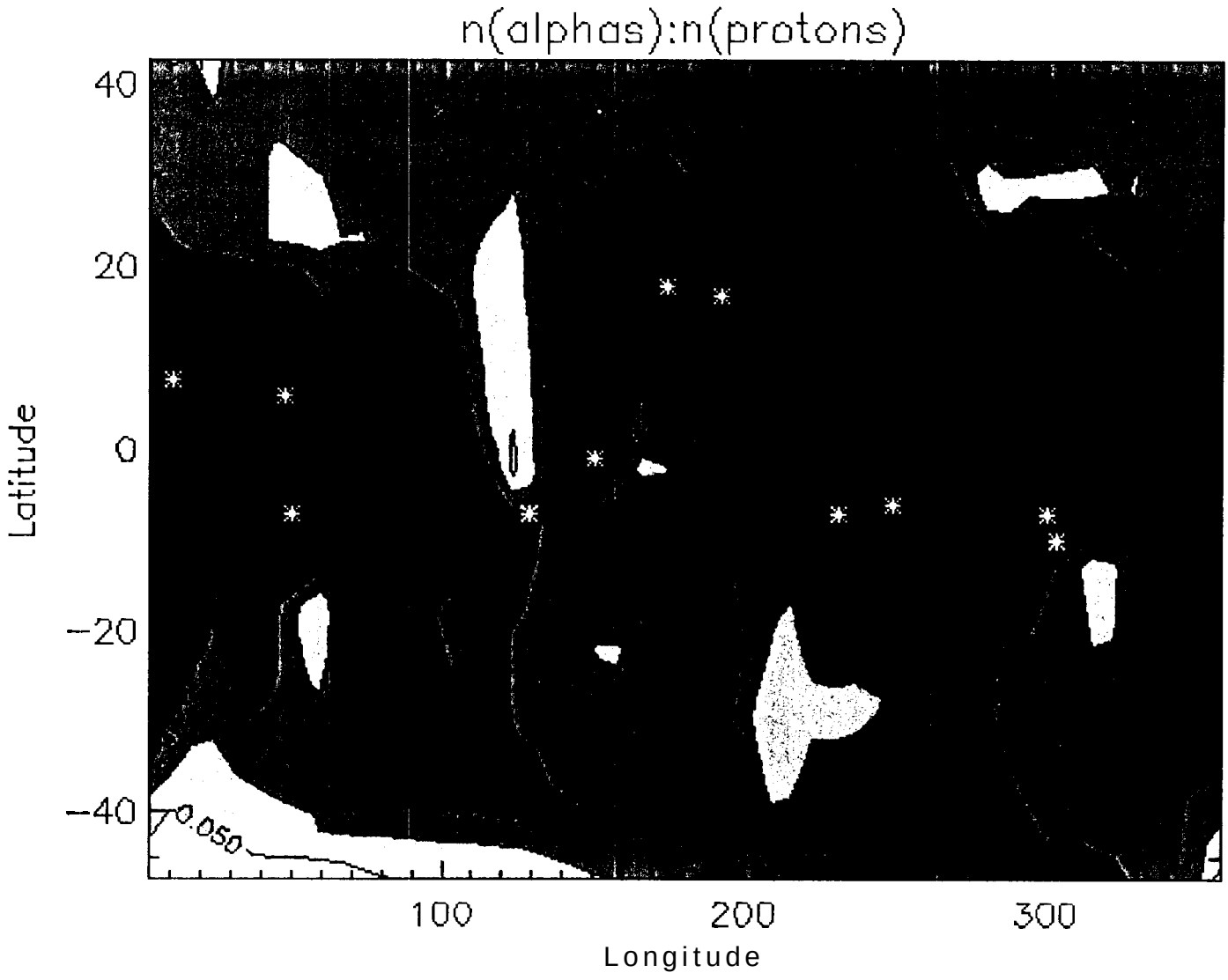
n(alphas):n(protons)
40
20
0
−20
−40
Latitude
0.050
100
200
300
Longitude

Fig 8b

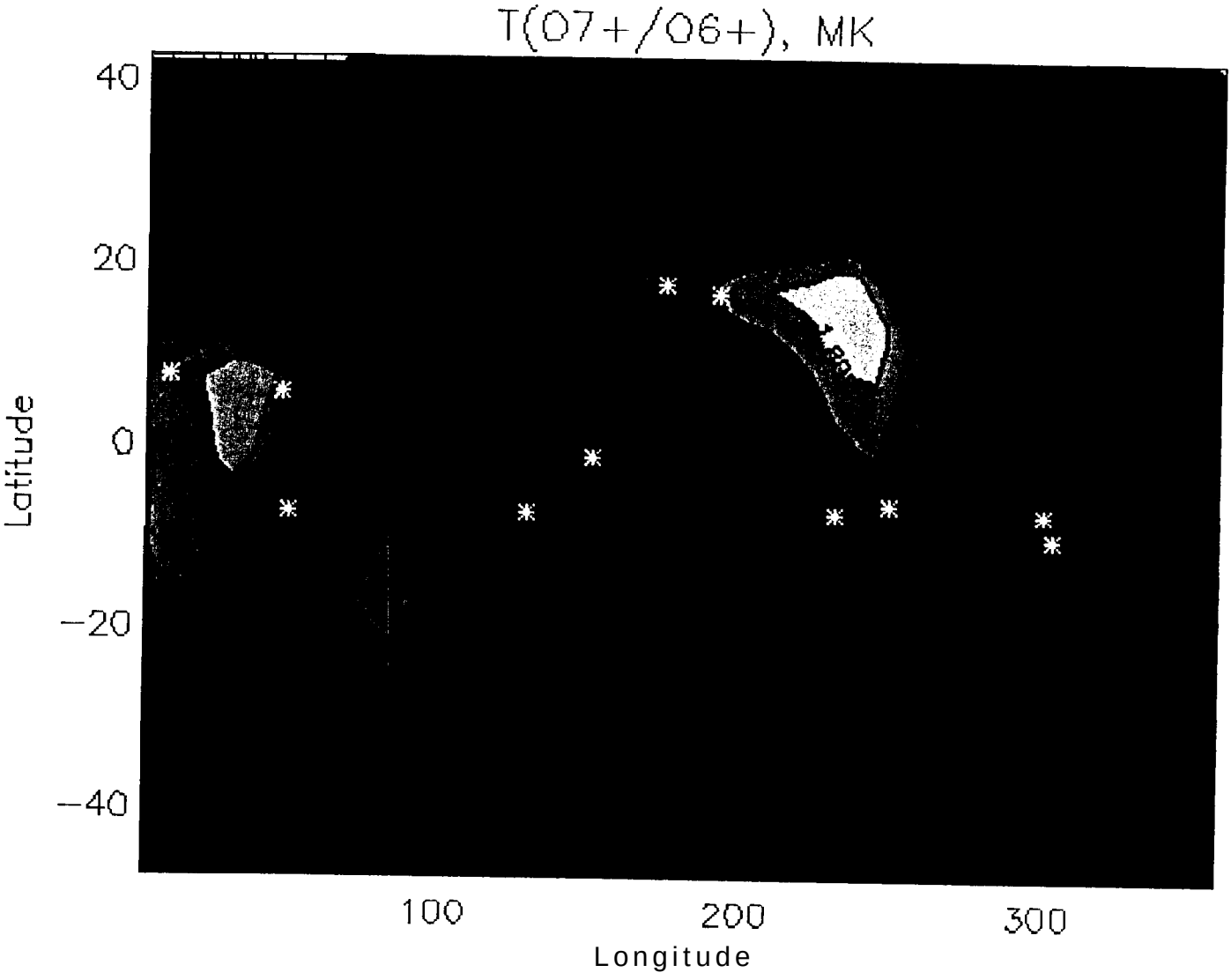

Fig 8c

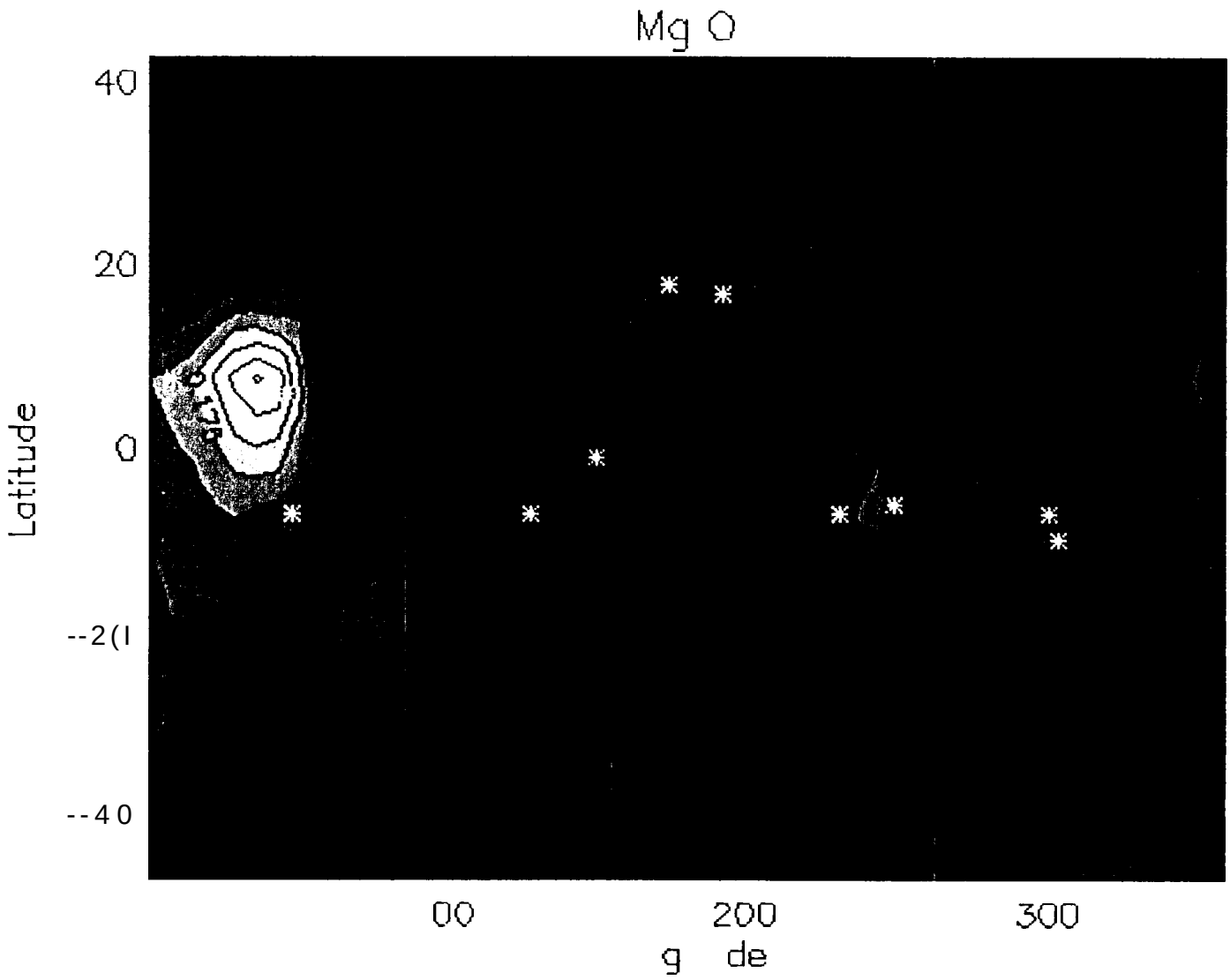

Fig 8d

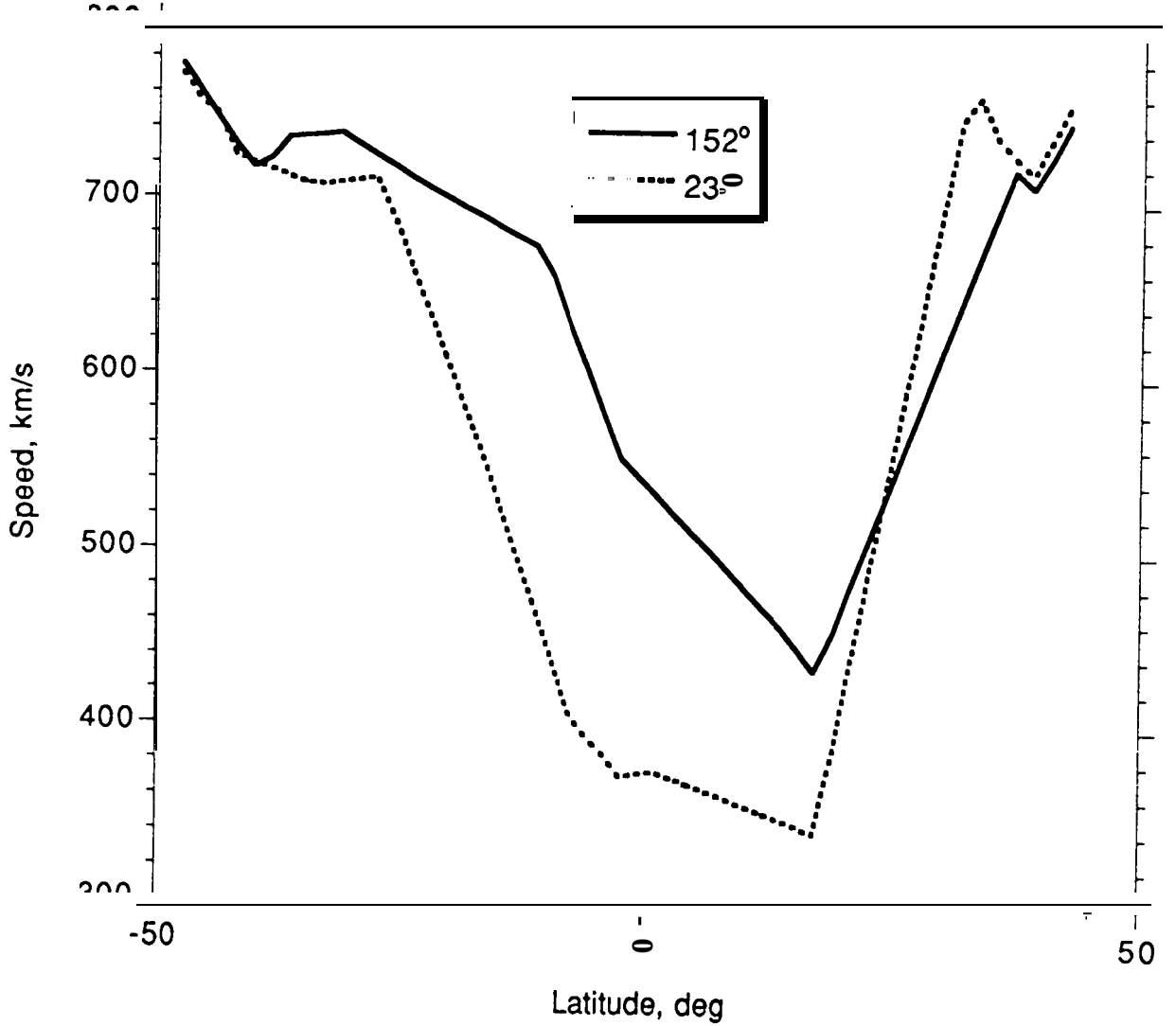

Fig 9

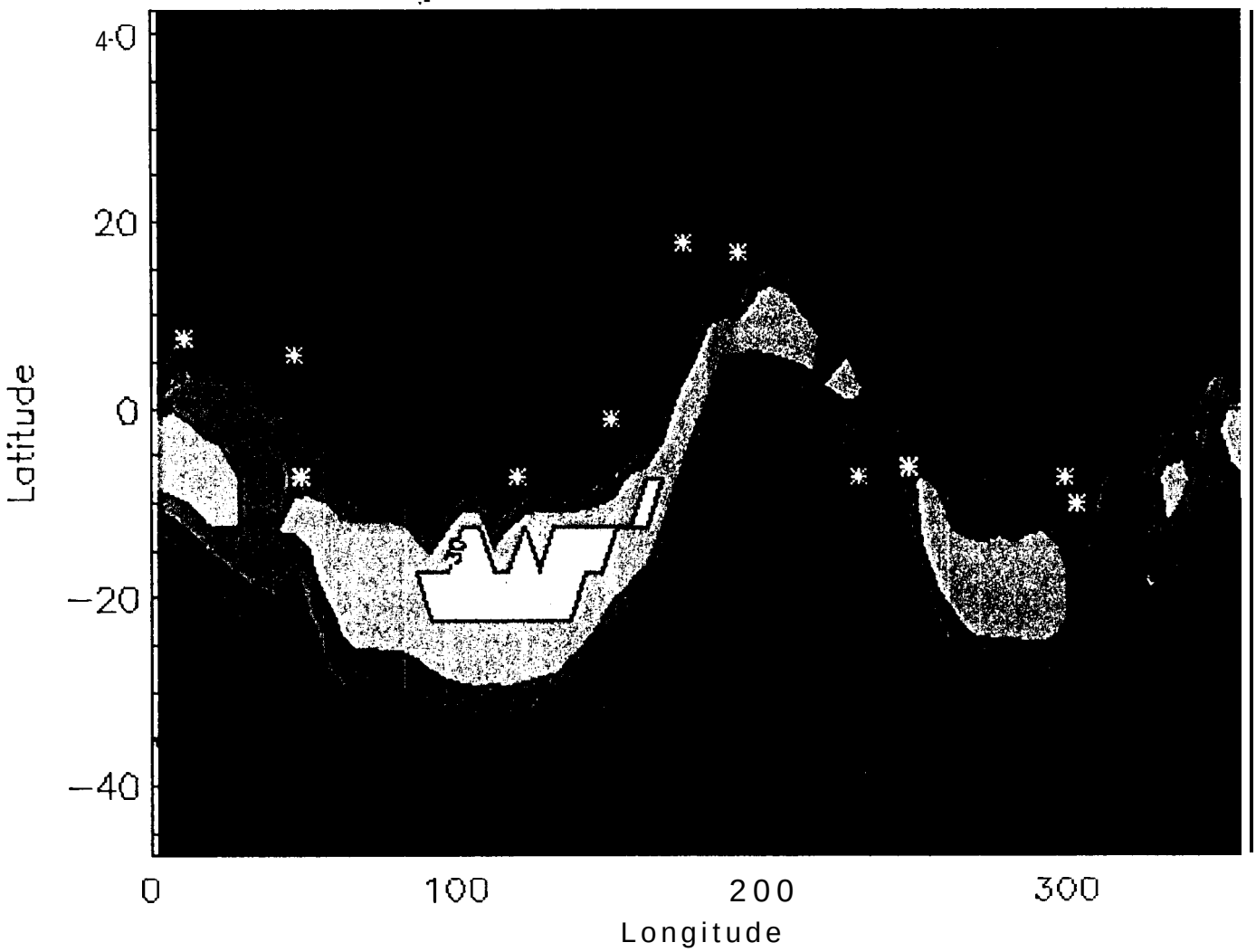
Expansion Factor, <1892--4>
40
20
0
−20
−40
Latitude
0
100
200
300
Longitude

Fig 10